ORIGINAL PAPER



Mesoscale metrics on approach to the clogging point

Grace Cai¹ · Anna Belle Harada¹ · Kerstin Nordstrom¹

Received: 21 July 2020 / Accepted: 15 June 2021 / Published online: 10 July 2021 © The Author(s), under exclusive licence to Springer-Verlag GmbH Germany, part of Springer Nature 2021

Abstract

In this work we present results of the flow of monodisperse spheres in a two-dimensional silo. By taking high-speed video during the flow of grains, we are able to look at the microscopic dynamics of the individual grains. We report on how measures such as velocity fluctuations, non-affine motion, and dynamical heterogeneities change in as the system approaches clogging. While we do find changes in these metrics on approaching the clogging point, we do not see evidence to suggest that it is a critical point. We contrast the clogging transition with the jamming transition in light of these results.

Keywords Silo flow · Clogging · Non-affine motion · Dynamical heterogeneity

1 Introduction

The flow and jamming of granular material has been studied for many years. With respect to flow, granular material is a truly complex fluid. In some instances the material can be modeled as a continuum fluid [1, 2]. However the realities of secondary flows, nonlocal effects, and boundary conditions can create real-world situations that evade modeling. The equivalent Navier–Stokes equations for granular flow have not been found. Nonetheless, recent continuum models such as nonlocal granular fluidity [3] have shown very promising results, even producing many of these secondary flow features that prove important in real flows.

The jamming of granular materials has also been extensively studied. This has commonly been called the jamming transition, and is easier to explain in the context of unjamming the system. A densely packed system of particles may become unjammed if the packing fraction is lowered, an external shear stress is applied, and/or the temperature is increased. (This could be the actual temperature if the particles are colloids, or a granular temperature (e.g. induced by vibration) for macroscopic particles.) This transition is associated with critical behavior in the system, including growing time and length scales. The jamming phase diagram, with axes of packing fraction, shear stress, and temperature has become iconic [4–6].

A very common system that exhibits both flowing and jammed states is a silo or hopper. However, the process for achieving the jammed state in a silo ("clogging") is distinct from the jamming transition mentioned previously. This distinction will be discussed further. In addition to its great practical importance in many industrial processing situations, it also displays a number of intriguing flow characteristics. Recently, interest in these systems has increased due to advances in technology making such systems quantifiable in new ways. Advances in computing and high-speed imaging have made it possible to study the microscopics of these flows [7–9], and techniques such as MRI and CT scanning have been employed [10, 11]. Many have also become quite interested in the connections between silo flow and other kinds of bottleneck flows, such as pedestrian egress and traffic bottlenecks [12–14].

Before moving on, we make a distinction between clogging and jamming here. "Jamming" will refer to the notion of passing through a boundary of the jamming phase diagram, which presumes an isotropic infinite system in the zero shear rate limit. Clogging refers to the formation of a permanent blockage at the outlet in a silo flow. While a clogged state is indeed a jammed state (mechanically rigid) it did not achieve that state via a jamming transition. For instance, the system does not uniformly become clogged: it is a local event, perhaps just five particles create the clog, and the state itself is produced by particle motion, not its absence.

While there is an obvious mechanistic distinction, we are interested (as are others [15, 16]) in what else distinguishes



Mount Holyoke College, South Hadley, MA, USA

clogging from jamming, or in finding other commonalities. Are there similar signatures upon the approach to clogging, like a growing dynamic length scale? Is there an equivalent clogging phase diagram [15], with modified control parameters? For clogging it is proposed that there are three somewhat analogous control parameters. The first is a length scale (the ratio of aperture size to particle size) which arguably takes the place of packing fraction. The second is the "compatible load"—the driving force behind the flow, which arguably takes the place of the external shear stress. Lastly, the temperature variable is replaced by an "incompatible load," some feature like vibrations that might suppress clogging.

Further, even though continuum models may reproduce overall behavior in these systems, we may be interested practically in the experiences of individual particles, or local neighborhoods of particles. If the connection to panicked pedestrian egress is made, it becomes obvious why we should care about individual experiences. However, this is important practically for real flows. If some particles never make the exit this may imply some segregation in the flow, which is typically undesired in an industrial setting, not to mention the buildup of product that doesn't outflow, perhaps creating new bottlenecks. The local experiences of particles, such as locking and shearing at contacts, may also influence how much they are damaged in the flow process.

In this paper, we study a quasi-2D silo flow. We focus on free-flow behavior, and approach the clogging point by reducing the aperture size. Using high-speed video, we are able to report on several particle/mesoscale behaviors in the flow as the clogging point is approached: velocity fluctuations, non-affine motion, and dynamical heterogeneities. These metrics are defined in the corresponding sections. We compare these results with measurements in systems approaching the jamming point.

2 Methods

2.1 Experiment

We study the flow of monodisperse spheres in a quasi-2D silo. The silo walls are transparent to allow imaging of the particle motions. The particles are clear acrylic spheres (Engineering Labs). They are highly monodisperse, with a diameter of $d=3.160\pm0.002$ mm, sampled by micrometer measurement. The size distribution skews to the smaller size, with no particles sampled exceeding 3.175 mm. For each experiment, we start with a filled silo, which is approximately 12,000 particles. The particles are poured into the top of the apparatus for each experimental run, and completely emptied before pouring for new experiments. The front and back of the silo is made with 3/8-in. static dissipative acrylic

sheets (McMaster-Carr). Teflon sheeting (McMaster-Carr) was laser cut (Epilog) to make inserts to provide the appropriate sidewall and aperture geometry. For different aperture sizes, a different insert is used. The insert is sandwiched between the acrylic sheets. The sheets and inserts have tapped holes, and so the silo is screwed together with set screws. The silo is then mounted onto a support frame built from t-slot aluminum, which rests on an optical table. The resulting dimensions of the silo are: 200 mm wide, 475 mm tall, and 3.2 mm thick. Before a trial, testing is done with a rod of fixed diameter to ensure the gap is sufficient to allow free flow of particles, and in rare cases of any doubt, the set screws are all loosened the same small amount. This process is iterated until the gap is judged sufficient. Plugs to close the aperture while filling the silo were 3D printed (Makerbot) to specification, allowing the particles on the plug to rest flush with the other particles on the bottom. The plugs are primarily flat pieces that are inserted horizontally, and designed to be removed via a swift horizontal motion, minimizing their influence on the outflow dynamics. Specifically, if one considers the silo area to be the xy-plane, the plug is inserted/ removed in the z direction. A force sensor (Pasco) is placed below the aperture to measure the mass flow rate. We use a Phantom v1611 camera (Vision Research) to film flow at 1000 frames per second at a resolution of 1280×800 pixels. The system is illuminated by symmetric LED spotlights to the sides of the camera. This results in bright reflections at the center of each particle. These reflections are used for tracking. Tracking is done via homebuilt code in MATLAB, which is an adaptation of the Crocker-Grier code [17], which gives subpixel accuracy of particle positions.

Before moving on, a note about the choice of monodisperse particles. Monodisperse particles in 2D do show some regions of crystallization. We have chosen to follow the path of other groups, which is to simply go ahead with it. In other words for spherical grains in 2D silos, it has been standard practice to look at monodisperse grains. This is a very practical choice, as different grain sizes would create additional 3D structure in the gap between walls. Small particles might settle down into the crevices between large grains and be "in front" or behind them. (As a digression, this is reminiscent of the Ising model on a hexagonal lattice.) However, results from many groups with spherical particles have consistently appeared to match the behavior of 3D grains, which are much less likely to crystallize even if monodisperse. So while it is interesting to think about experiments without any crystallization, this is future work. For instance, crystallization can be suppressed by using bidisperse disks, which our group is also doing work towards.



2.2 Simulation

We perform simulations in LAMMPS (lammps.sandia.gov) with the "granular" package. The particle interactions are given by a Hertzian interaction with Coulomb friction ("pair style gran/hertz/history") and interact normally and tangentially with each other [18]. Properties are tuned to match the acrylic spheres in the experiments. The particles also experience a uniform gravitational field. The simulations are run much like the experiments. Particles are poured into a quasi-2D box of dimensions 200d in height, 63.3d in width, and 1.1d in depth (d = particle diameter), settle the particles, create an outlet at the center of the silo base, and let particles exit the silo. These box dimensions correspond to our experimental setup. Note that the box is only thick enough to fit one layer of spherical particles.

Due to the controlled nature of the simulations, which do not naturally contain randomness as experiments do, the simulations produce the same results in identical initial conditions. For repeated simulation runs, we introduce variability into the system by placing a fixed intruder into the silo before particles are poured. The intruder itself is made of particles bonded together permanently. The intruder diameter is about 10 particle diameters and is placed above the aperture, at various heights but at a minimum distance of 30d above the opening. This has been shown to be far enough to not influence the exit [19], even if the intruder were to remain. Before initiating flow, the intruder particles are deleted from the simulation, and the remaining particles are allowed to settle into place, and extra particles are poured into the top as needed. This intruder protocol creates a different initial packing structure before the flow is initiated. We have confirmed that this procedure does not influence the flow rate or avalanche size systematically. Avalanche size is measured by the number of particles that flow out of the silo, from the initiation of flow until the formation of a stable arch. Flow rate is measured by the number of particles that outflow per second (Fig. 1).

3 Bulk results

To begin, it is important to show our system behaves as it should. The general phenomenology of gravity-driven silo flow is simple. There appears to be a transitional exit aperture size, about five grain diameters. The precise value varies from system to system, but the phenomenon is general. When the exit aperture is larger than this transitional size, particles will flow continuously according to the Beverloo law, with a rate that is independent of filling height, provided the fill height is adequate and the silo width is large enough compared to the aperture and grain diameters [20].

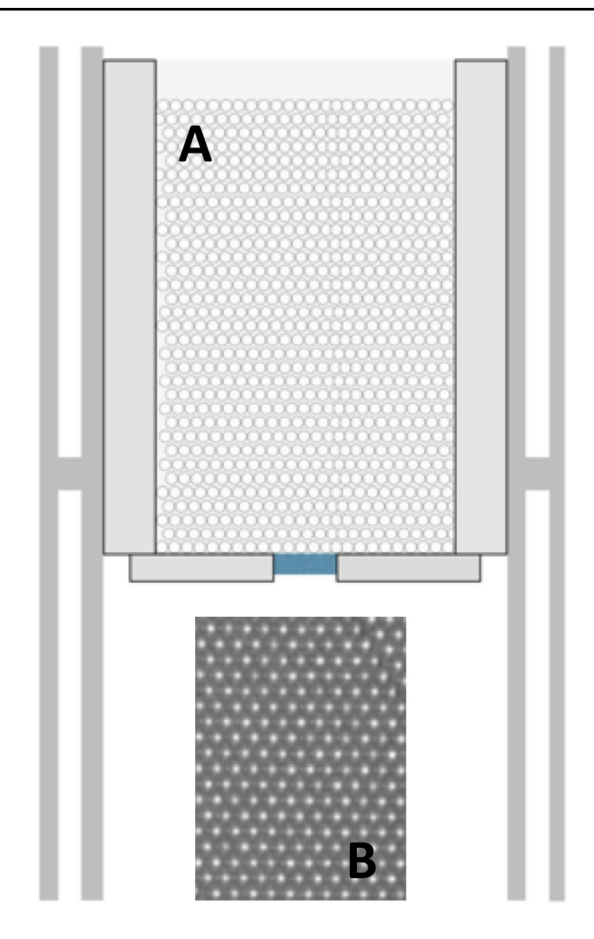


Fig. 1 a A schematic of the silo used in our experiments, with relative proportions modified for clarity of presentation. A monolayer of grains is poured between two acrylic sheets. The gap between the sheets as well as the exit aperture are set by a Teflon insert sandwiched between the acrylic sheets. The apparatus is supported by aluminum framing. b An image of particles in our flow experiments. The bright spots are reflections off the particle centers used for tracking. The particles themselves are close-packed in this image, though may take on a more disordered configuration in the general case

This precise flow rate will vary slightly from system to system, but the functional form holds over a wide array of systems. When the aperture is smaller than this transitional size, particles will form a clog with some likelihood [21, 22]. In the infinitely tall silo limit this means any silo with a small aperture will clog eventually. There is no way to predict when this clog will occur, but larger aperture sizes will have larger average discharge events before a clog [23]. There is controversy in the literature about whether the transition in behavior marks a critical point, or whether the clogging transition is simply probabilistic in nature: beyond some aperture size, it becomes overwhelmingly unlikely for a clog to occur [24–27].

Silo flow for apertures above the clogging size is almost always described well by the Beverloo equation for silo flow [28]. The Beverloo equation in 2D is as follows:



69 Page 4 of 11 G. Cai et al.

$$W = C\rho_B \sqrt{g}(R_A - kd)^{3/2} \tag{1}$$

In this equation W is the mass flow rate per unit time, ρ_B is the bulk density of the granular material, g is the acceleration due to gravity, R_A is the size of the aperture, and d is the particle size. C and k are empirical fit coefficients, though generally k is of order 1. Note that W does not depend on time, on the filling height of the silo, nor on any obvious material parameters aside from density. In 3D the main qualitative change is the size of the exponent (5/2).

The equation can be divided through by the mass of one particle m_p , to recover an equivalent expression for the particle flow rate, \dot{N} . One can also factor out the particle size from the parenthetical factor in Eq. 1. We define R as the nondimensional aperture size: $R = R_A/d$. Absorbing the prefactors into a constant A, the expression for the particle flow rate reduces to this simple expression:

$$\dot{N} = A(R - k)^{3/2} \tag{2}$$

We present results of experiments for systems that free-flow, with exit aperture diameters 5d, 6d. 7d, 8d, 10d and 20d, where d is the diameter of one particle. It should be noted that while 6d rarely clogs, 5d has a high clogging probability of 73% [29]. Results presented here are for trials where clogging does not occur, with three trials for each aperture size. As show in Fig. 2 we see good agreement with experiments, simulation, and the 2D Beverloo equation.

We take statistics on avalanches using the simulation for R < 5, as it is experimentally untenable to do the equivalent experiments and build up good statistics. It takes a long time to reset and refill the apparatus, and the smaller aperture sizes run into issues of uncertainty in aperture size,

whereas the simulation does not have such uncertainties. Avalanche size s is defined as the number of particles that outflow before a clog forms, and we sample 100 runs for each value of R. One form proposed for the dependence of average avalanche size on R is given by [23]:

$$\langle s \rangle = Be^{\alpha R^2} - 1 \tag{3}$$

In this expression α , B are constants related to the probability one particle will pass through the aperture without forming an arch. Thus a plot of $\ln(\langle s \rangle + 1)$ vs R^2 should yield a straight line. We see that this captures our data well in Fig. 3. The basis for this form is based on the idea that clogging is a random process. The R^2 dependence of the exponent is directly related to geometry, in 3D this form becomes R^3 . We have tested this data against other models [24], including those incorporating a critical aperture size, but we find this form fits the data best. While we do not dwell in particular on this result, we see that this lends more weight to the idea that clogging is not connected to a critical outlet size.

4 Velocity fields and fluctuations

Next, we consider the particle motions. In our trials during free flow, we take videos of the flow and use particle tracking methods to reconstruct trajectories for the particles, as detailed further in the experimental section. Specifically, we are able to measure instantaneous position and velocity of each particle. One simple visualization is show in Fig. 4 for R = 5 and R = 20 for about 1 second of developed flow. Each particle's position is marked by one pixel, and we overlay the position for subsequent frames on the image, to see the

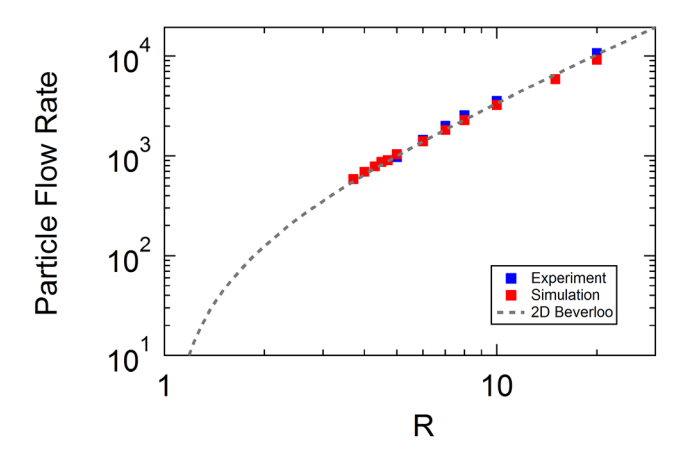


Fig. 2 Particle flow rate data as a function of aperture size from our experiments and simulations, fit to the Eq. 2 version of the Beverloo equation. The fit shown is to $\dot{N} = 124(R-1)^{3/2}$. k is fixed at 1 for the fit, and $A = 124 \pm 5$. For this nonlinear fit, the data are weighted according to their experimental uncertainties

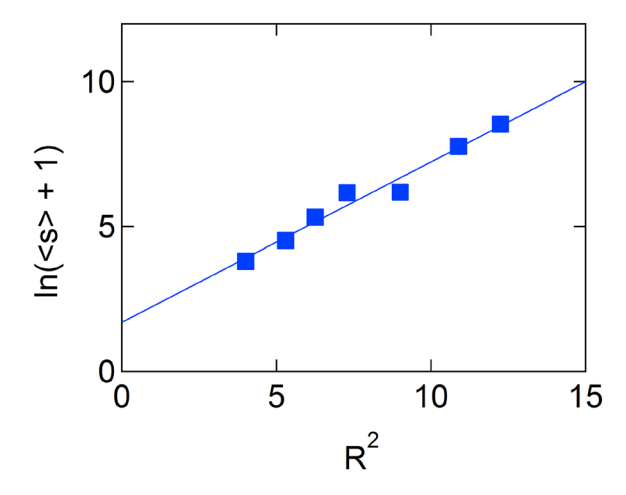
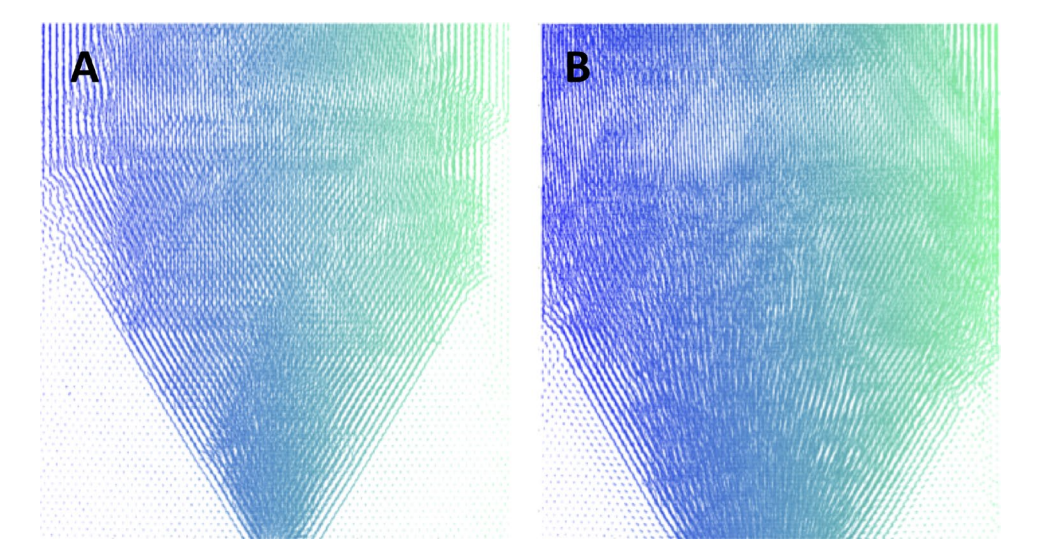


Fig. 3 Average avalanche size dependence on aperture size R. What is plotted is $\ln(\langle s \rangle + 1)$ vs R^2 , to show agreement/disagreement with Eq. 3. The fit is to a line, with (intercept) $B = 1.69 \pm 0.354$ and (slope) $\alpha = 0.554 \pm 0.0424$



Fig. 4 a A plot of particle tracks for R = 5 for about 1 second of flow. The tracks are colored by their horizontal position in the first frame analyzed, to aid in visualizing the flow. b The same plot as in (a) for R = 20

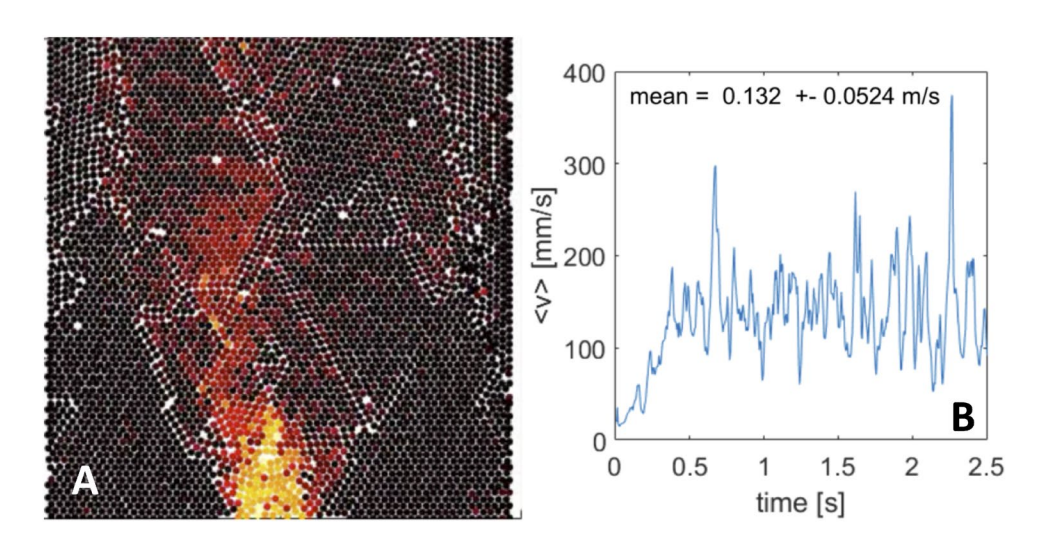


trajectories. The colors are simply a guide to the eye, and indicate the initial horizontal position of each particle. This visualization also suggests some mixing within the system, but that is future work, beyond the scope of this paper. Using this visualization, we see that particles near the edge may never make it out, and that the R = 20 particles have a much more pronounced direct downward flow through the aperture. The R = 5 data is more jagged, showing regions of halting and plastic deformations.

We also observe spatiotemporal inhomogeneity in the flows. Figure 4 shows some asymmetry in between the left and right side (note that this is for 1 s of data) in both examples. This was indeed a consistent observation, using this high time resolution. However, the asymmetry would not persist: we would see that one side would move faster than the other, then the sides would switch. This effect was more pronounced for smaller apertures. This was difficult to fully characterize, we have also observed this to a greater effect with flows involving an obstacle [29]. We show a qualitative example of this in Fig. 5a for R = 5, where particles are colored by instantaneous speed.

Regardless of the spatial structure of the flow, we see that the particle speed itself has a well-defined average, but is quite unsteady in time. Figure 5b shows a representative example of this, showing the average speed from the initiation of flow through 2.5 s (the total outflow time is a factor of 10 larger for this aperture). This shows a transient development of about 0.5 s, then an unsteady, but developed average speed. The average are taken in the bottom portion of the silo (a roughly square area of 600×650 pixels) across all particles for each time. We also do not see any signature of a clogging event in plots of speed vs time. The graph up until the clog is indistinguishable from a system that doesn't clog: there are fluctuations and then a very abrupt stop, and the abrupt stop looks no different from a regular dip in the plot. However, we might ask how the fluctuations themselves change with

Fig. 5 a A map of the particle speed for one frame of one R = 5 experiment. The particles are colored by their speed, with the warmest colors at the highest speed, and black is no/very little motion. Asymmetry in the instantaneous velocity field is apparent. b Average instantaneous speed vs time for the same experiment. Each datapoint is the average over all particles within the bottom portion of the silo. The overall mean speed is shown (color figure online)





changing aperture size in free-flow conditions. This is the question we explore next.

To characterize the velocity fluctuations more precisely, we find the average speed during developed flow for each experiment, and then calculate each particle's instantaneous difference from that speed: $\delta v = v - v_{ave}$. This data is accumulated for all particles in all frames, in the bottom portion of the silo, and we find the standard deviation of this data. This is a similar method to [30], however we have used the actual speed (magnitude of total velocity) rather than just the horizontal speed (magnitude of horizontal component). We are also measuring the deviation from the long-term average, rather than the instantaneous average. Nonetheless, this is enough to show a clear trend with changing aperture size. We plot the results for all experiments in Fig. 6. The (relative) velocity fluctuations grow on approach to the clogging point, in agreement with results of [27, 30]. However, the "clogging point" for this experiment is somewhere around 6 particle diameters, and R = 5 is an aperture size that definitely clogs. Were this to be a phase transition point, we might expect a sharp increase (e.g. a peak) in the velocity fluctuations at the transition—though the details of this would depend on the order of the transition. But there is no kink or any other feature in the graph near our potential critical point that indicates this is a special point; there is no signature of transition. The slight misordering of R = 7 and R = 8 is not statistically significant.

5 Non-affine motion

The velocity fluctuations are measurable, but this does not give insight into how the particles move. In order for some particles to outflow, some other particles must get stuck or

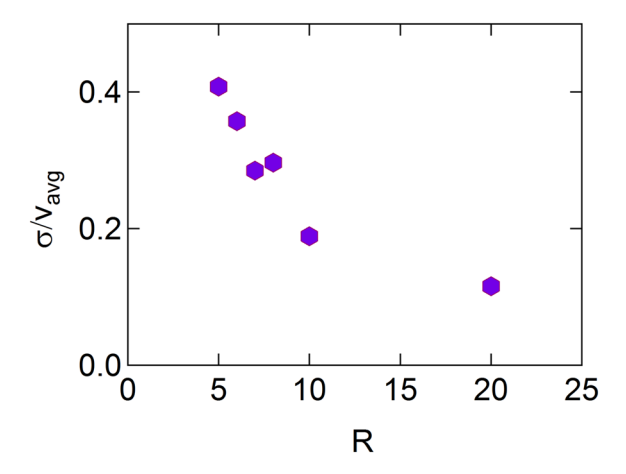
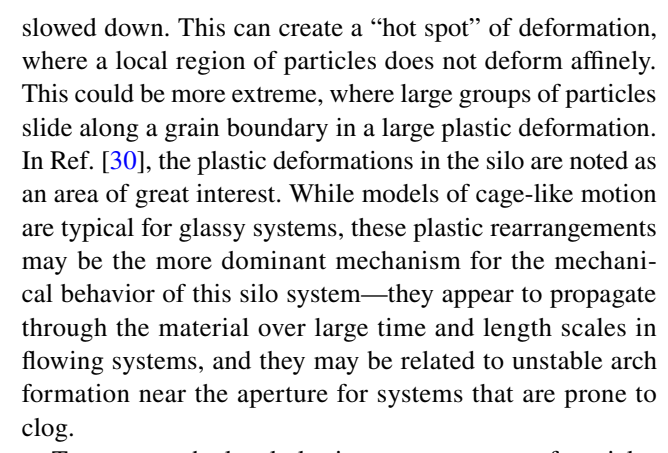


Fig. 6 The dependence of velocity fluctuations on aperture size. Fluctuations are measured by the standard deviation of the parameter $\delta v = v - v_{avg}$, normalized by v_{avg} , where v is a single particle speed at a single time. The fluctuations group as the aperture size gets smaller



To measure the local plastic rearrangements of particles relative to their neighbors in the silo flow, we use the metric D_{min}^2 [31]:

$$D_{min,i}^{2} = min \left\{ \sum_{j} \left[\Delta \bar{d}_{ij}(t) - E_{i} \bar{d}_{ij} \right]^{2} \right\}$$
 (4)

This metric quantifies the nonaffine deformation of the j particles in the neighborhood around a given particle i after removing the averaged linear response to the strain, given by the tensor E_i . The vector \bar{d}_{ij} is the relative position of i and j, $\bar{d}_{ij}(t)$ is the relative displacement after a delay time t. This method removes the macroscopic flow from the calculation of non-affine motion [31–33]. In more detail, the linear strain tensor is not known in advance, it is the best fit to the actual deformation; the algorithm minimizes the difference between the actual deformation and the calculated deformation by sampling values of E_i .

The j particles used to calculate D_{min}^2 are typically chosen to be within approximately 2d of the reference particle i for amorphous systems. We restrict this radius to be 1.5d as our particles are packed tightly. Every particle has a value of D_{min}^2 for every chosen delay time between frames. D_{min}^2 has an embedded lengthscale and timescale. Low values of D_{min}^2 indicate the motion is likely affine in that region, whereas high values indicate plastic deformations or other rearrangements.

For our data, we measure D_{min}^2 for all experiments for two different delay times: dt = 2 frames and dt = 10 frames during developed flow. One burning question parallels our investigation into velocity fluctuations: is there a signature in the fluctuations of D_{min}^2 preceding a clog? However, much like the velocity, we do not find any such signature preceding a clog, but we illustrate the fluctuations in the average value in Fig. 7.

We show representative frames of this measurement for two aperture sizes R = 5 and R = 20 in Fig. 8. We see that R = 20 for dt = 2 shows little non-affine motion (Fig. 8C), but the equivalent plot for R = 5 (Fig. 8a) shows what appears to be more small regions of high D_{min}^2 . Moving



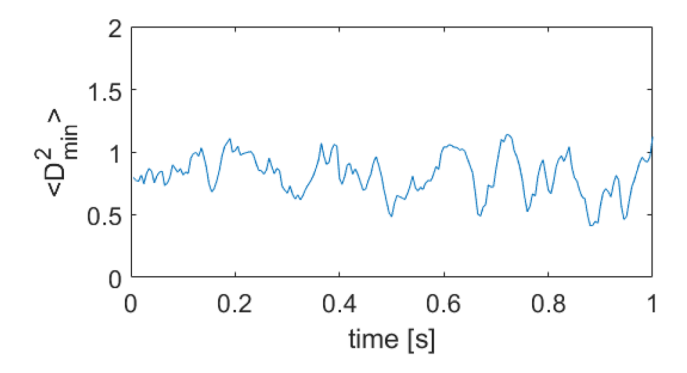


Fig. 7 Fluctuations in the average value of D_{min}^2 for dt = 2 frames. The data is shown for R = 5 for one second of fully-developed flow

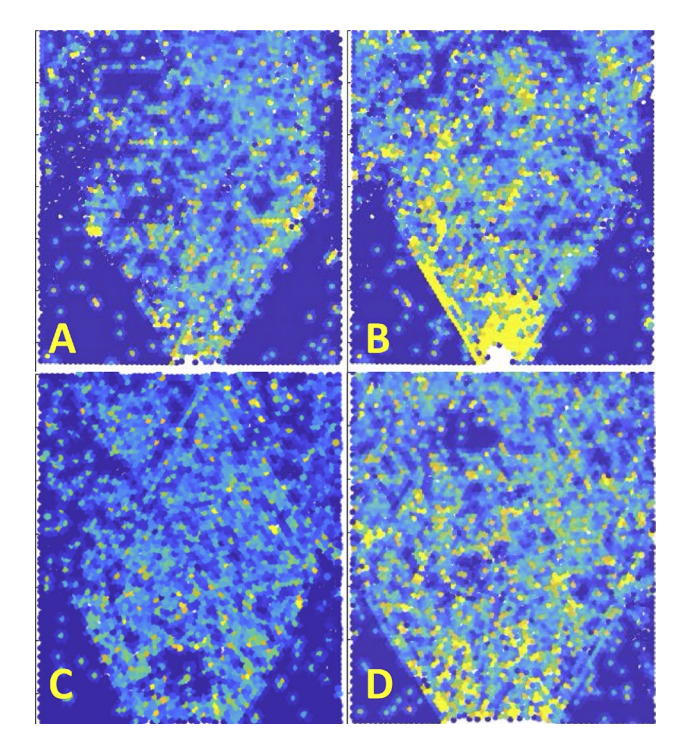


Fig. 8 Snapshots of D_{\min}^2 in the silo for various experiments and delay times. **a** R = 5, dt = 2, **b** R = 5, dt = 10, **c** R = 20, dt = 2, **d** R = 20, dt = 10. Yellow corresponds to higher values of D_{min}^2 , blue corresponds to low values (color figure online)

over to plots 8B and 8D, we see that a larger timescale produces more non-affine motion, which is not surprising. However the contrast between the two aperture sizes becomes more apparent. The larger aperture has non-affine motion distributed somewhat randomly through the flowing region, with a stronger signal near the exit. The smaller aperture also has an increased value near the exit, but shows distinct larger regions of non-affine motion in the bulk, including a visible large plastic deformation at a grain boundary on the left (Fig. 8b).

The visual perception of a higher D_{min}^2 may be misleading, so we calculate the mean D_{min}^2 value for each aperture size for all experiments, in the same region used for velocity measurements. First we calculate the average value for dt = 2. For comparison between apertures, we divide the average value of D_{min}^2 by the average displacement squared for dt = 2, which we denote Δr^2 . This makes D_{min}^2 dimensionless, though with an associated timescale. While the rescaled D_{min}^2 is not numerically equivalent to the proportion of non-affine motion compared to the total motion, it does represent this proportion, in that it will monotonically increase as the proportion of non-affine motion grows.

Next we consider the relative sizes of the rescaled D_{min}^2 values for different aperture sizes. In Fig. 9, the data is plotted. We see a clear (black circles) increase in nonaffine motion as the aperture size gets smaller. For the dt = 10data (red circles), we rescale the data by the same Δr^2 and then divide by $\sqrt{5}$ as this should be the proper adjustment for delay time scaling [31]. We see the data collapse for both values of dt, indicating we do not appear to be probing significantly different dynamics for the two delay times.

6 Dynamical heterogeneities

The transition to jamming in granular and colloidal systems is accompanied by the growth of dynamical heterogeneities [34, 35]. As the system is typically closely packed, a grain must cooperate with its neighbors in order to move. String-like swirling motions or "conga lines" of particles may be observed if one can see the particles. The closer the system is to jamming, whether it is smaller strain rate, a

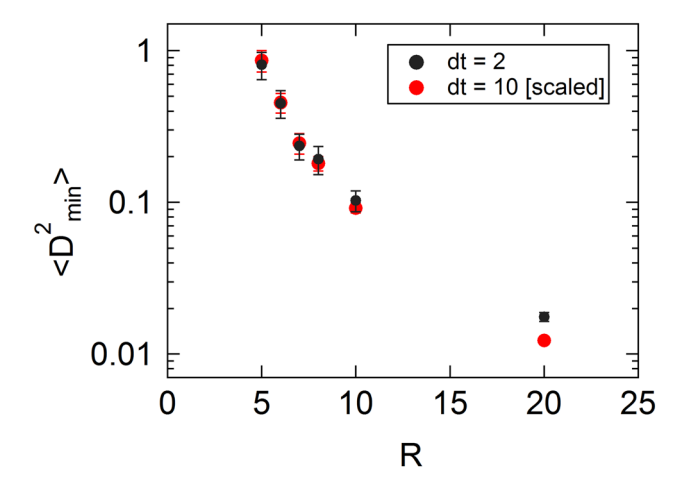


Fig. 9 The dependence of the average value of D_{min}^2 as a function of dimensionless aperture size. D_{min}^2 values for dt = 2 (black circles) have been rescaled by the average displacement squared for the same time interval, and dt = 10 (red circles) have been rescaled for collapse (color figure online)



higher packing fraction, or a lower temperature, these collective motions are larger, and thus a growing length scale is reported on approach to jamming. Additionally, these cooperative motions become rarer, and a growing timescale may also be measured.

To look into the cooperative motions in the silo flow, we turn to an often used metric in the jamming and glass community to characterize these dynamics, the quantity χ_4 , which measures dynamical heterogeneities. To define χ_4 , we first define the simple self-overlap order parameter $w_i(\tau)$, which compares a particle's position in two frames. If the particle has not moved more than a cutoff distance (typically the particle size), then $w_i = 1$, if the particle has moved more, then $w_i = 0$ for that particle and delay time combination. Then an ensemble average is taken over all particles for a given start time to get the order parameter Q, defined as so:

$$Q(t,\tau) = \sum_{i} w_{i}(t,\tau)$$
 (5)

Here t refers to the start time and τ is the delay time. In the absence of any heterogeneous dynamics, Q would resemble w exactly. However, due to heterogeneous dynamics, there are fluctuations in the instantaneous number of fast moving regions which manifests as a variability in the decay of $Q(t,\tau)$ for different start times. By computing the variance of this decay for different start times, the heterogeneity may be quantified. It is customary to multiply this variance by the number of particles N, to form a metric that does not depend on N as the variance for counting statistics will go as 1/N. This is the parameter χ_4 , also called the dynamic susceptibility:

$$\chi_4(\tau) = N[\langle Q(\tau)^2 \rangle_t - \langle Q(\tau) \rangle_t^2] \tag{6}$$

0.8 0.6 0.4 0.2 0 0 0.5 1 1.5 2

 τ [s]

Fig. 10 a The particle averaged self-overlap order parameter (colors) displayed for different start times. The average with respect to start times is overlaid on top (thick black line). The curve does not decay to zero as there are particles that never move. **b** The normalized vari-

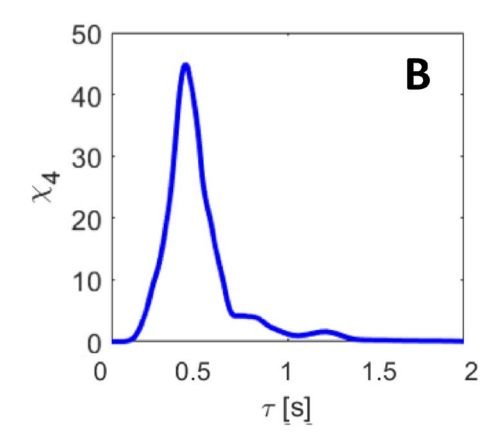
We illustrate a typical procedure for the calculation of χ_4 in Fig. 10 for experimental data R=5. Fig 10a shows the Q order parameter functions overlain for a number of different start times, and the average over start times is shown. Note that our data does not decay to zero, as there are some particles that do not move. However, the decay curve shows a clear plateau and looks as expected. For systems with heterogeneous dynamics, the function χ_4 should have a peak value (χ_4 *) at some time (τ *). By calculating the variance as described in Eq. 6, we generate Fig. 10b, and clearly see a peak.

A counting argument [36] gives the number of grains n * in a dynamical heterogeneity:

$$n *= \frac{\chi_4 *}{(Q_1 - Q_0)(Q_1 - Q *)} \tag{7}$$

Here Q * is the value of Q where χ_4 is maximized, and Q_1 and Q_0 are the average contributions from the fast and slow regions. The quantities Q *, Q_1 and Q_0 will all be between zero and one, and not in generally dramatically different from one another. Thus the value of n * will be some fixed multiple of χ_4 *, of order 1-10 [37]. We will report the value of χ_4 * only, but bring this up to acknowledge that it connects to a physical length scale for cooperative motion.

In Fig. 11, we show results for all of our experiments. Figure 11a shows the value of χ_4 * vs R, and we see that this value grows as the aperture size grows. We also see in Fig. 11b that the value of τ * does not systematically change, as far as we can tell. These are somewhat surprising results, as jammed systems tend to have time and lengthscales that grow together. However, to our knowledge this is the first measurement of such a parameter in this type of system. We discuss these results in the next section.



ance of Q, which is χ_4 . A clear peak is seen. The height of the peak corresponds to a lengthscale for cooperative motion, and the peak location corresponds to a timescale (color figure online)



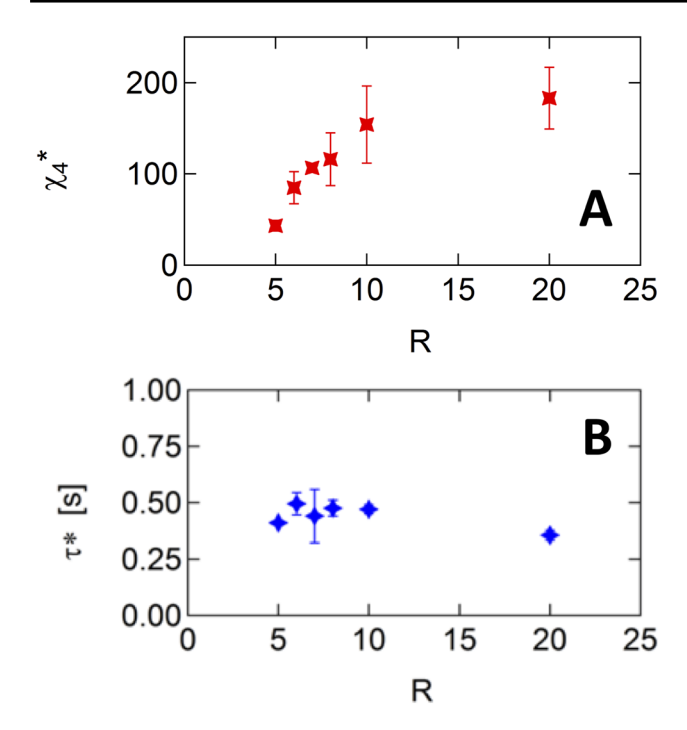


Fig. 11 a χ_4 * vs R for all experiments. The error bars represent the spread in measured values. Clearly, the value increases as R increases. **b** $\tau * vs R$ for all experiments. There is no apparent trend in this data

7 Discussion

The results of fluctuation measurements agree with prior results from silo flows [27, 30] and indicate higher relative fluctuations as the clogging point is approached. This also qualitatively agrees with findings regarding systems approaching the jamming point [38], where fluctuations increase approaching this point. However, the similarities end there. The contrast with jamming comes with the nature of the increase, where fluctuations are specifically found to diverge. We see no divergence of the fluctuations, just a smooth growth with decreasing aperture size, and our data includes one aperture with a high clogging probability. Were there to be some transition point, we would see it.

For "uncooperative" motions in systems, D_{min}^2 has been shown to increase on approaching the critical density from above [5]. That is, if a system of soft particles starts above the jamming point, non-affine responses to external stresses will grow as the packing fraction is reduced. This makes some sense from an intutive standpoint, as there is more space for particles to rearrange. We find that the D_{min}^2 parameter increase on approaching the clogging point. In one sense this might appear to be the same finding, but requires thinking through the analogy. For our system, apertures far from the clogging point actually represent systems with more free space, the packing is reduced. Thus the values of D_{min}^2 are not just a simple question of free space, it is competition between geometric frustration and a macroscopic driving flow. The presence of non-affine motion is more important for systems near the clogging point.

Another analogy might be between D_{min}^2 and shear rate, as in some granular systems D_{min}^2 has been shown to grow with shear rate $(\sim \dot{\gamma})$ [32]. However, we see the opposite trend here: higher overall shear rates correspond to larger apertures, and the clear direction is the other way. A true comparison would compare D_{min}^2 values to the local shear rates, and indeed this is current work.

An open question involves the contribution of different types of non-affine motion. There are local hotspots, larger failures along a grain boundary, and perhaps something else unimagined. One other contribution to non-affine motion will be due to granular temperature: particles will experience random fluctuations due to collisions, and these motions would register as non-affine. This would be especially relevant near the outlet.

For cooperative motions, we see that the cooperativity length increases with aperture size. For jammed systems, one sees this lengthscale grow as the shear rate is decreased [37], and generally grow on approaching the jamming density [34]. We see the opposite effect in general, as aperture size increases, the length scale increases. Increasing the aperture size drives the system away from jamming in a classical sense: there is more free space and a higher shear rate. This is a very intriguing result. One point to remember is that for jammed/near-jammed systems, the strain rate is uniform or zero. Here the strain rate is not uniform, and the particles near the center seem to form streamlines downwards more, especially for larger apertures. This may be a large component of the cooperative motions.

We also see that the timescale does not appreciably change, whereas for jammed systems this grows on approach to jamming. We hypothesize that for silo flow, this timescale is set by fixed system parameters, such as gravity and perhaps the sound speed. While these are difficult to check experimentally, it would be worth exploring these effects via simulation.

While we have characterized D_{min}^2 as indicating "uncooperative" motion and χ_4 as indicating "cooperative" motion, it should be noted they are not opposite metrics. The presence of a string of particles moving faster than average might require nonaffine motions at its edges. A large clump of rearrangement will involve cooperation. Thus seeing opposite trends in the two metrics is especially intriguing. Future work will involve characterizing the regions of cooperative motion, as they are typically thought to be stringlike, but may be "clumpy" in some circumstances [35].

We have presented measurements of mesoscopic dynamics in a granular system on approach to the clogging point, one for cooperative motion and one for uncooperative motion. We see that these metrics change, but in ways that



require further investigation, and show that the clogging point is different in many ways from the jamming point. Practically, a strength of these metrics is that while they are built from particle-scale data, and report on mesoscale behavior, the average values report the system changes effectively, thus they may be useful bulk monitors. (Temperature is another example of a metric built on microscopics that is a useful system monitor.) Unfortunately, our experimental measurements cannot uncover the microscopic mechanisms of the phenomena we have observed. In the case of D_{min}^2 , a natural extension is to test the dependence of the D_{min}^2 value on the local strain rate. Further, there are different potential modes of non-affine deformations, so it would be worth characterizing them and their relative importance. What causes these non-affine motions? It may take looking into the interparticle forces [39] to gain ultimate clarity. For the χ_4 parameter, the data is even more "smeared" as not only are all particles averaged over, but the function itself does not have a value at a particular time point—it requires averaging over multiple time points. However, these cooperative motions do exist, so locating and categorizing them is the next challenge. Lastly, while we do not find evidence for a true clogging transition, it is worth exploring the notion of the clogging phase diagram [15] further, by exploring these metrics in systems of different granular temperatures, perhaps by adding vibrations.

Acknowledgements The authors thank Emma Thackray for helpful discussions, and Leonard McEachern and Thomas Liimatainen for technical support. This work is partially funded by ACS PRF Award 56888-UN19, by the Research Corporation for Science Advancement Award 24516, and by NSF CAREER Award 1846991.

Declarations

Conflict of interest The authors have no conflicts of interest to declare that are relevant to the content of this article.

References

- Staron, L., Lagrée, P.Y., Popinet, S.: The granular silo as a continuum plastic flow: the hour-glass vs the clepsydra. Phys. Fluids 24, 103301 (2012)
- 2. Staron, L., Lagrée, P.Y., Popinet, S.: Continuum simulation of the discharge of the granular silo. Eur. Phys. J. E **37**(1), 5 (2014)
- 3. Kamrin, K.: Quantitative Rheological Model for Granular Materials: The Importance of Particle Size, pp. 1–24. Springer (2018)
- Liu, A.J., Nagel, S.R.: Jamming is not just cool any more. Nature 396(6706), 21 (1998). https://doi.org/10.1038/23819
- van Hecke, M.: Jamming of soft particles: geometry, mechanics, scaling and isostaticity. J. Phys.: Condens. Matter 22(3), 033101 (2009)
- O'Hern, C.S., Silbert, L.E., Liu, A.J., Nagel, S.R.: Jamming at zero temperature and zero applied stress: the epitome of disorder. Phys. Rev. E 68, 011306 (2003). https://doi.org/10.1103/PhysRevE.68.011306

- Kondic, L.: Simulations of two dimensional hopper flow. Granul. Matter 16, 234 (2014)
- 8. Hong, X., Kohne, M., Morrell, M., Wang, H., Weeks, E.R.: Clogging of soft particles in two-dimensional hoppers. Phys. Rev. E **96**, 062605 (2017)
- Janda, A., Zuriguel, I., Maza, D.: Flow rate of particles through apertures obtained from self-similar density and velocity profiles. Phys. Rev. Lett. 108, 248001 (2012)
- Stannarius, R., Sancho Martinez, D., Finger, T., Somfai, E., Börzsönyi, T.: Packing and flow profiles of soft grains in 3D silos reconstructed with X-ray computed tomography. Granul. Matter 21(3), 56 (2019)
- Fullard, L., Holland, D.J., Galvosas, P., Davies, C., Lagrée, P.Y., Popinet, S.: Quantifying silo flow using MRI velocimetry for testing granular flow models. Phys. Rev. Fluids 4, 074302 (2019)
- Pastor, J.M., Garcimartín, A., Gago, P.A., Peralta, J.P., Martín-Gómez, C., Ferrer, L.M., Maza, D., Parisi, D.R., Pugnaloni, L.A., Zuriguel, I.: Experimental proof of faster-is-slower in systems of frictional particles flowing through constrictions. Phys. Rev. E 92, 062817 (2015)
- Helbing, D., Buzna, L., Johansson, A., Werner, T.: Self-organized pedestrian crowd dynamics: experiments, simulations, and design solutions. Transp. Sci. 39(1), 1 (2005)
- Helbing, D., Johansson, A., Mathiesen, J., Jensen, M.H., Hansen,
 A.: Analytical approach to continuous and intermittent bottleneck flows. Phys. Rev. Lett. 97, 168001 (2006)
- Zuriguel, I., Parisi, D.R., Hidalgo, R.C., Lozano, C., Janda, A., Gago, P.A., Peralta, J.P., Ferrer, L.M., Pugnaloni, L.A., Clément, E., Maza, D., Pagonabarraga, I., Garcimartín, A.: Clogging transition of many-particle systems flowing through bottlenecks. Sci. Rep. 4, 7324 (2014)
- Péter, H., Libál, A., Reichhardt, C., Reichhardt, C.J.O.: Crossover from jamming to clogging behaviours in heterogeneous environments. Sci. Rep. 8(1), 10252 (2018)
- Crocker, J.C., Grier, D.G.: Methods of digital video microscopy for colloidal studies. J. Colloid Interface Sci. 179(1), 298 (1996)
- Zhang, H.P., Makse, H.A.: Jamming transition in emulsions and granular materials. Phys. Rev. E 72, 011301 (2005)
- Zuriguel, I., Janda, A., Garcimartín, A., Lozano, C., Arévalo, R., Maza, D.: Silo clogging reduction by the presence of an obstacle. Phys. Rev. Lett. 107, 278001 (2011)
- Nedderman, R., Tuzun, U., Savage, S., Houlsby, G.: Simulations of two dimensional hopper flow. J. Chem. Eng. Sci. 37, 1597 (1982)
- To, K., Lai, P.Y., Pak, H.K.: Jamming of granular flow in a twodimensional hopper. Phys. Rev. Lett. 86, 71 (2001)
- To, K.: Jamming transition in two-dimensional hoppers and silos. Phys. Rev. E 71, 060301 (2005)
- Janda, A., Zuriguel, I., Garcimartín, A., Pugnaloni, L.A., Maza,
 D.: Jamming and critical outlet size in the discharge of a twodimensional silo. EPL (Europhys. Lett.) 84(4), 44002 (2008)
- Thomas, C.C., Durian, D.J.: Geometry dependence of the clogging transition in tilted hoppers. Phys. Rev. E 87, 052201 (2013)
- Zuriguel, I.: Invited review: clogging of granular materials in bottlenecks. Pap. Phys. 6, 060014 (2014)
- Thomas, C.C., Durian, D.J.: Fraction of clogging configurations sampled by granular hopper flow. Phys. Rev. Lett. 114, 178001 (2015)
- Thomas, C.C., Durian, D.J.: Intermittency and velocity fluctuations in hopper flows prone to clogging. Phys. Rev. E 94, 022901 (2016)
- 28. Mankoc, C., Janda, A., Arevalo, R., Pastor, J.M., Zuriguel, I., Garcimartin, A., Maza, D.: The flow rate of granular materials through an orifice. Granul. Matter **9**(407), 10252 (2007)



- Harada, A.B., Nordstrom, K., Zuriguel, I., Garcimartin, A., Cruz, R. (eds.): Traffic and Granular Flow 2019, pp. 365–371. Springer (2020)
- Zuriguel, I., Maza, D., Janda, A., Hidalgo, R.C., Garcimartín,
 A.: Velocity fluctuations inside two and three dimensional silos.
 Granul. Matter 21(3), 47 (2019)
- Murdoch, N., Rozitis, B., Nordstrom, K., Green, S.F., Michel, P., de Lophem, T.L., Losert, W.: Granular convection in microgravity. Phys. Rev. Lett. 110, 018307 (2013)
- Utter, B., Behringer, R.P.: Experimental measures of affine and nonaffine deformation in granular shear. Phys. Rev. Lett. 100, 208302 (2008)
- Chen, D., Semwogerere, D., Sato, J., Breedveld, V., Weeks, E.R.: Microscopic structural relaxation in a sheared supercooled colloidal liquid. Phys. Rev. E 81, 011403 (2010)
- Keys, A.S., Abate, A.R., Glotzer, S.C., Durian, D.J.: Measurement of growing dynamical length scales and prediction of the jamming transition in a granular material. Nat. Phys. 3, 260 (2007). https:// doi.org/10.1038/nphys572
- Zhang, Z., Yunker, P.J., Habdas, P., Yodh, A.G.: Cooperative rearrangement regions and dynamical heterogeneities in colloidal

- glasses with attractive versus repulsive interactions. Phys. Rev. Lett. **107**, 208303 (2011). https://doi.org/10.1103/PhysRevLett. 107.208303
- Abate, A.R., Durian, D.J.: Topological persistence and dynamical heterogeneities near jamming. Phys. Rev. E 76, 021306 (2007)
- Katsuragi, H., Abate, A.R., Durian, D.J.: Jamming and growth of dynamical heterogeneities versus depth for granular heap flow. Soft Matter 6, 3023 (2010)
- Woldhuis, E., Chikkadi, V., van Deen, M.S., Schall, P., van Hecke, M.: Fluctuations in flows near jamming. Soft Matter 11, 7024 (2015)
- Thackray, E., Nordstrom, K.: Gravity-driven granular flow in a silo: characterizing local forces and rearrangements. EPJ Web Conf. 140, 03087 (2017)

Publisher's Note Springer Nature remains neutral with regard to jurisdictional claims in published maps and institutional affiliations.

